



Asymmetric packaging of polymerases within vesicular stomatitis virus [☆]



Jeffery Hodges ^{a,b}, Xiaolin Tang ^{a,b}, Michael B. Landesman ^{a,b}, John B. Ruedas ^c, Anil Ghimire ^a, Manasa V. Gudheti ^{d,g}, Jacques Perrault ^c, Erik M. Jorgensen ^{e,g}, Jordan M. Gerton ^{a,f}, Saveez Saffarian ^{a,b,g,*}

^a Dept. of Physics and Astronomy, University of Utah, United States

^b Center for Cell and Genome Science, University of Utah, United States

^c Dept. of Biology, San Diego State University, United States

^d Vutara, Inc., Salt Lake City, UT, United States

^e Howard Hughes Medical Institute, United States

^f Dept. of Bioengineering, University of Utah, United States

^g Dept. of Biology, University of Utah, United States

ARTICLE INFO

Article history:

Received 4 September 2013

Available online 19 September 2013

Keywords:

VSV
RdRP
Polymerase
PALM
STORM
AFM
L protein
P protein
Viral replication

ABSTRACT

Vesicular stomatitis virus (VSV) is a prototypic negative sense single-stranded RNA virus. The bullet-shape appearance of the virion results from tightly wound helical turns of the nucleoprotein encapsidated RNA template (N-RNA) around a central cavity. Transcription and replication require polymerase complexes, which include a catalytic subunit L and a template-binding subunit P. L and P are inferred to be in the cavity, however lacking direct observation, their exact position has remained unclear. Using super-resolution fluorescence imaging and atomic force microscopy (AFM) on single VSV virions, we show that L and P are packaged asymmetrically towards the blunt end of the virus. The number of L and P proteins varies between individual virions and they occupy 57 ± 12 nm of the 150 nm central cavity of the virus. Our findings position the polymerases at the opposite end of the genome with respect to the only transcriptional promoter.

© 2013 The Authors. Published by Elsevier Inc. All rights reserved.

1. Introduction

Vesicular stomatitis virus (VSV) possesses a single-stranded negative sense RNA genome and is the prototypic model for understanding transcription and replication of potent human pathogens including Ebola and rabies. VSV is also an effective oncolytic agent since some attenuated VSV strains replicate preferentially in malignant cells [1]. Taken together, VSV is emerging as a useful model and potent tool in the arsenal of modern medicine.

VSV virions are 180 nm long and 80 nm wide and resemble a bullet with one tapered and one blunt end. The VSV genome is tightly encapsidated by nucleoprotein (N), forming the N-RNA genome template. Recent CryoEM studies showed N-RNA forms a left-handed helix that winds around a cavity, with the 3' end at

the tapered end and the 5' end at the blunt end [2–4] (please see corrections to ref 5 for the correct RNA orientation). Like all other non-segmented negative sense (NNS) RNA viruses, VSV packages multiple copies of a polymerase that consists of the L protein catalytic subunit (241 kDa) and a template-binding P protein subunit (30 kDa). The polymerases transcribe and replicate the N-RNA genome by engaging at promoter sites at or near the 3' end of the genome template [5].

On average ~50 L and ~400 P proteins are packaged within each virion [6]. The position of the L and P proteins within the bullet shaped virion has not been established previously. L organizes itself into a ring structure with an approximate diameter of 10 nm and does not bind the template by itself [7–9]. P proteins form dimers through their central domains and also bind L and the N-RNA template [8,10,11]. In recent CryoEM studies of VSV [3], either symmetry mismatches between the N-RNA helix, L and P, or random positioning of L and P, resulted in averaging out of the L and P density within the central cavity of VSV. Therefore to resolve the position of L and P, single virion imaging techniques with sufficiently high resolution are required.

While the resolution of simultaneously imaged multiple fluorophores is limited by diffraction, the position of a single fluorescent

[☆] This is an open-access article distributed under the terms of the Creative Commons Attribution-NonCommercial-No Derivative Works License, which permits non-commercial use, distribution, and reproduction in any medium, provided the original author and source are credited.

* Corresponding author at: Dept. of Physics and Astronomy, University of Utah, United States.

E-mail address: saffarian@physics.utah.edu (S. Saffarian).

molecule can be localized with nanometer precision. The precision of localization is inversely proportional to the square root of the number of photons collected from the single molecule [12]. It is therefore possible to reconstruct an image by successively photoactivating subsets of molecules that are further apart from each other than the diffraction limit and localizing their positions with nanometer precision. This principle was developed in photoactivatable localization microscopy (PALM, [13]) fluorescence photoactivatable localization microscopy (fPALM, [14]) and stochastic optical reconstruction microscopy (STORM, [15]) to achieve in plane resolutions of ~ 20 nm. The axial resolution of these techniques can be extended either through introduction of astigmatism associated with the out of plane images [16] or using Biplane imaging [17] both of which report an axial resolution of ~ 50 nm.

Although fluorescence is specific, it does not report the density of unlabeled protein molecules. Atomic force microscopy (AFM) is sensitive to the overall protein density, via changes in the mechanical properties of the sample: the protein density within an object can be probed by measuring the deformation of a sample in response to a force applied by the AFM cantilever. AFM has been used in this way to measure the stiffness of single virions [18–20]. In general, the non-enveloped viruses are very stiff with a Young's modulus in the range of GPa [20] while the enveloped viruses can be an order of magnitude softer in the range of 100 MPa [18].

Since the N-RNA is packaged with specific orientation of its 5' end at the blunt end of the virion [3] and since the polymerases can only engage a promoter at the 3' end [21,22], positioning of the polymerases within the bullet will inform our understanding of the early transcription of the N-RNA genome immediately upon delivery to the host cytoplasm and to some extent the final moments of packaging the genome in budding virions.

2. Materials and methods

2.1. Super-resolution imaging and fluorescence localization

Images were recorded with a SR 200 microscope (Vutara, Inc.) based on the Biplane approach [17]. The envelope of VSV virions was mapped by labeling $\sim 75\%$ of the VSV-G protein on the exterior of the virion with Alexa-Fluor[®]647 (Invitrogen A21245). Alexa fluorophores can be efficiently initialized to their dark state in imaging buffer [SI] and can then be photo-activated through

application of 405 nm UV light. This method was used to generate the viral envelopes shown in Figs. 1 and 2.

To locate the internal proteins within individual virions, we used recombinant viruses encoding enhanced Green Fluorescent Protein (eGFP) linked to the viral proteins P or L. In these recombinant viruses, all of the P or L proteins are respectively replaced by P linked to eGFP (eGFP-P) or eGFP linked to L (L-eGFP) and these viruses have been previously characterized [23,24]. The center of mass of the eGFP labeled proteins was determined in each virion and its relative distance to the center of the high resolution envelope was measured. The eGFP proteins associated with these internal proteins were not photoswitched, rather their total fluorescence intensity and the position of their center of fluorescence with respect to the center of the envelope was determined.

Excitation and activation of single fluorescent molecules was achieved via a speckle-free illumination with an even intensity distribution, which was realized by a specialized beam homogenizer. Two color channels were detected sequentially at 50 frames/s. eGFP data was collected first over 500 frames at 30% power (1.2 kW/cm^2), then Alexa 647 was collected over 15,000 frames at 100% power (4 kW/cm^2). Data analysis was performed using the Vutara SRX software (Version 4.01).

2.2. Validation of super-resolution imaging method

First we have validated the resolution of the Biplane microscope by imaging beads on the microscope for 1000 imaging frames with an average fluorescence signal of 500 photons (comparable to our sample fluorescence). The analysis of this data as shown in detail in (SI) shows that we can localize these beads with less than 10 nm precision in XY and 25 nm precision along the optical axis. Resolution of the microscope is defined by the full width half maximum analysis and is 20 nm in plane and 50 nm along the optical axis.

Since the VSV G proteins are uniformly distributed on the surface of the envelope, we used them for our control experiments. VSV virions were pseudotyped with eGFP linked to the C terminus of VSV G protein (SI). Since virions are assembled on different cells within the population with varying levels of expression of VSV G-eGFP expression, the collected virions have a distribution of G-eGFP incorporation between virions. Each virion incorporates 1200 copies of G independent of whether the G has a GFP tag or not and G proteins are uniformly distributed on the surface of each virion [6]. We expect that the center of fluorescence of G-eGFP to

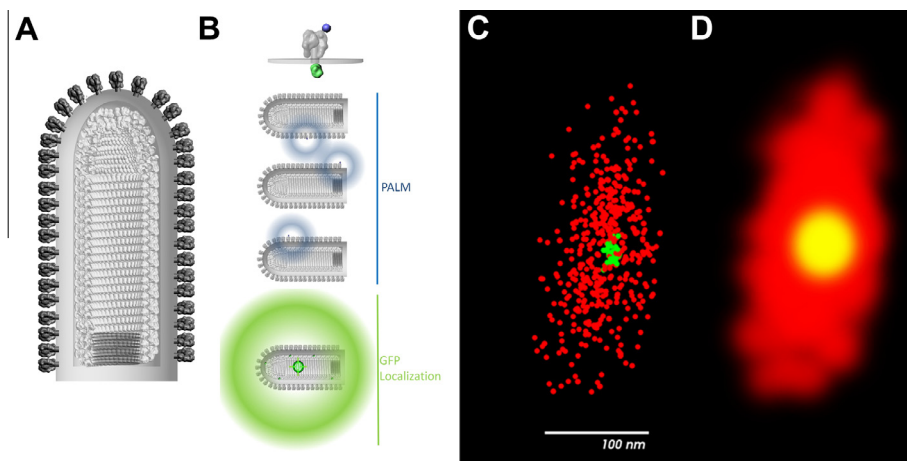


Fig. 1. Locating eGFP center of fluorescence within reconstruction of VSV envelope. (A) A model of VSV virion constructed partly from CryoEM data [3]. (B) VSV-G is tagged from the exterior with Alexa 647 and internally with eGFP, ensuring that the eGFP center of fluorescence coincides with the center of the virion. (C) Super-resolution fluorescence microscopy results in localization of VSV-G proteins (Red) and location of the center of fluorescence of eGFP (green). (D) Volumetric rendering of the VSV envelope from super-resolution fluorescence imaging data along with the location of the center of fluorescence of eGFP. (For interpretation of the references to colour in this figure legend, the reader is referred to the web version of this article.)

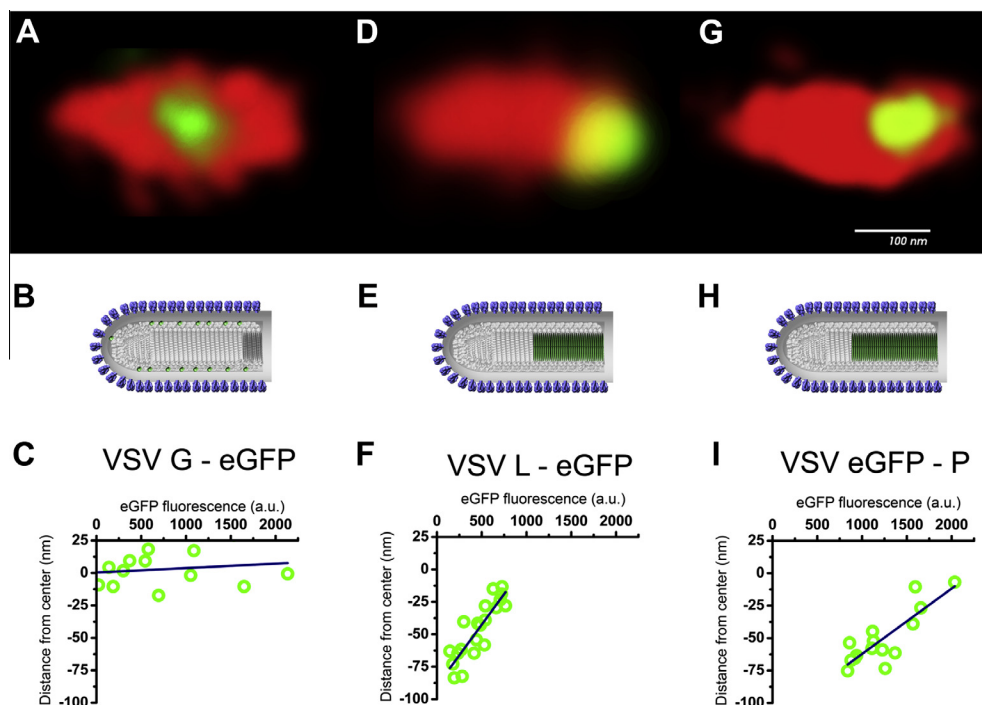


Fig. 2. Center of fluorescence of the eGFP-linked proteins (G, P, and L, respectively A, D and G). Images in the center (B, E, and H) show the model of the VSV constructed partly from CryoEM data [3] in comparison to representative volumetric rendering of virions (Red) and G-eGFP, eGFP-P, and L-eGFP (Green). The center of fluorescence of eGFP is shown in green. At the bottom (C, F, and I), the distributions of the center of fluorescence of the virions with respect to the amount of eGFP fluorescence detected from each virion shows packaging with a constant density. (For interpretation of the references to colour in this figure legend, the reader is referred to the web version of this article.)

co-localize with the center of the viral envelope independent of the number of G-eGFP proteins packaged on the surface of the virion. Because the virus is pseudotyped on a population of cells with varying expression levels of G-eGFP (SI), we also expect that the amount of G-eGFP in each virion will vary. As Figs. 1 and 2(A)–(C) show, the G-eGFP center of fluorescence overlapped with the center of the virion to within ± 11 nm, measured for 13 VSV:G-eGFP virions.

We also verified this method on HIV virions. HIV forms spherical virions with a diameter of 120–150 nm [25]. The membrane of these virions is coated internally with a lattice of Gag proteins as observed through CryoEM. The Gag lattice is uniformly distributed inside the virions with the exception of a few gaps [26], therefore we expect that the center of mass of Gag be very close to the center of the virion, if not exactly on the center of virions due to the possible empty patches. We verified our super-resolution fluorescence imaging method on HIV Virus Like Particles (VLPs) pseudotyped with VSV G which incorporated Gag-eGFP proteins (SI). G proteins were labeled with Alexa 647 tagged antibodies to mark the envelope of the VLP and 12 HIV virions pseudotyped with G incorporating Gag-eGFP showed that the center of the virion co-localized with the center of the Gag signal to within 12 nm precision as shown in (SI).

2.3. AFM materials and methods

We used atomic force microscopy (AFM) for iso-force scans across the surface of several virions. The AFM (Asylum Research MFP-3D in a dark environmental chamber) consists of a pyramidal gold-coated tip (radius of curvature ≈ 20 nm; height ≈ 10 μ m) attached to the underside of a pliable cantilever (force constant ≈ 3 N/m; length = 200 μ m), a piezoelectrically actuated sample scanner (<1 nm precision), and associated digital control and data acquisition electronics. On stiff samples, the AFM cantilever bends easily to accommodate changes in the sample height, so

the path of the tip faithfully reports sample topography. When the sample is more pliant than the cantilever, the sample will deform under the force of the tip, so the height signal becomes more indicative of the sample's stiffness rather than its topography, therefore, the height signal provides an iso-force map of the sample surface rather than a true topographical map.

3. Results

3.1. Super-resolution fluorescence imaging shows P and L are localized at the blunt end of VSV

To measure the center of mass of P and L proteins within the virus, we used recombinant viruses encoding enhanced Green Fluorescent Protein (eGFP) linked to the viral proteins P or L. In these recombinant viruses, all of the P or L proteins are respectively replaced by P linked to eGFP (eGFP-P) or eGFP linked to L (L-eGFP) and these viruses have been previously characterized [23,24]. VSV:L-eGFP is temperature sensitive, replicates in 32 $^{\circ}$ C and packages 1/3 of the wild type levels of the polymerase L. VSV:GFP-P grows at 37 $^{\circ}$ C to a lower titer than WT and packages half the L and P proteins when compared to WT virus. These fluorescent viruses although imperfect, allow localization of their L and P. Later, we will examine the effect of protein density on localization by comparing these viruses to WT using AFM.

The total fluorescence intensity detected from the virions is directly proportional to the copy number of packaged eGFP linked proteins; however, it cannot be used as an absolute measure of the copy number due to fluorescence quenching at high concentrations. More importantly for this work, the center of fluorescence of the eGFP pinpoints the center of mass of the L or P protein distributions, which can be determined with ~ 10 nm precision [12].

For all 15 VSV:eGFP-P virions measured, the eGFP-P center of fluorescence was located toward the blunt end of the virion. We observed a 30% variation in the total fluorescence between

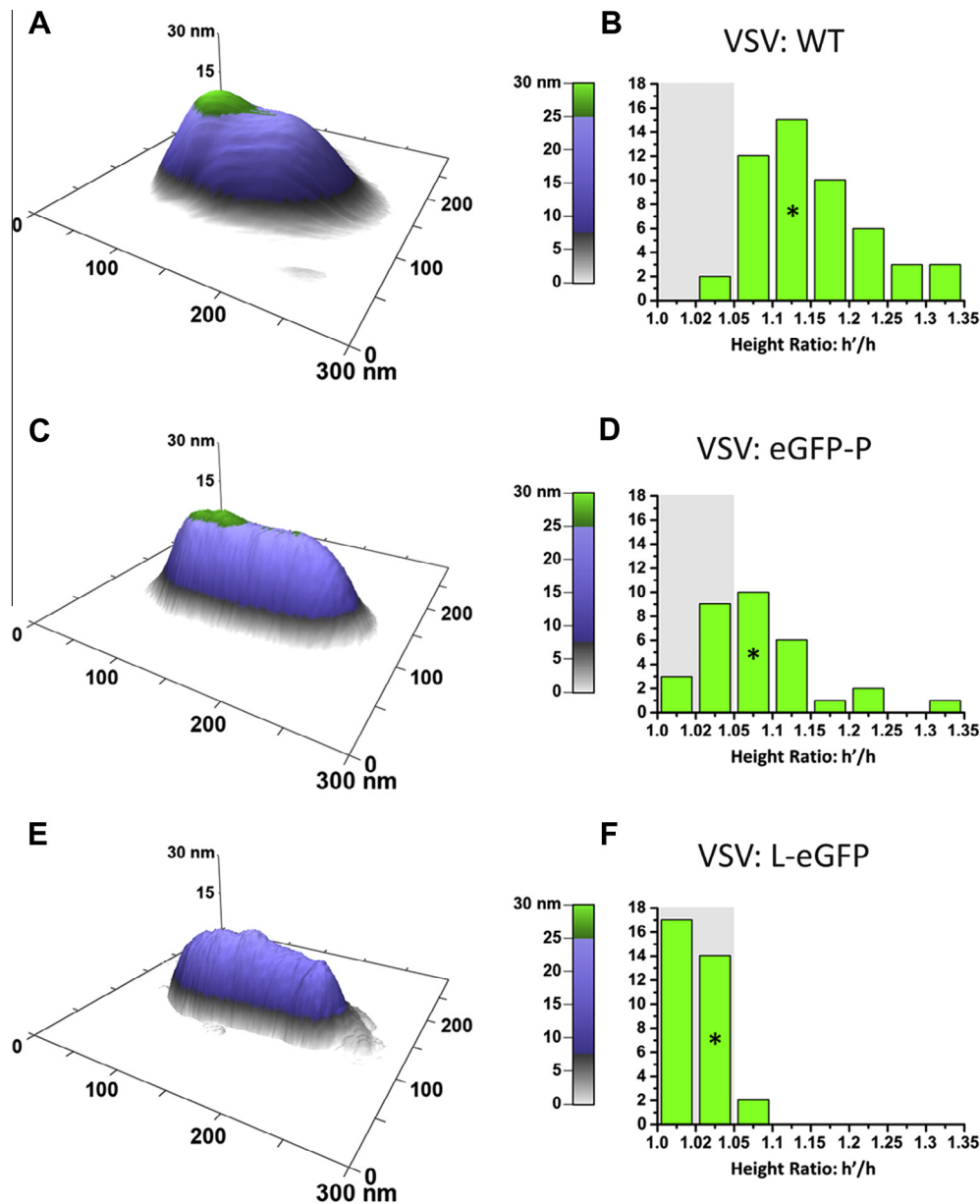


Fig. 3. AFM surfaces of VSV show two distinct regions with respect to structural composition, specifically a variation in elastic response to the force exerted by the tip. (A) Wild type VSV virions have the stiffest bump region, indicated by the tallest bump. (B) The ratio of the two regions' respective heights (h' for the bump, h for the main body) is 1.14 ± 0.07 for 50 WT virions. (C) A representative VSV:eGFP-P virion with a similarly distinctive bump. (D) VSV:eGFP-P h'/h is 1.07 ± 0.06 for 30 virions. (E) VSV:L-eGFP virions have little or no distinguishable regions towards the rear, and (F) have a measured h'/h of 1.02 ± 0.01 for 30 virions. *Indicates the representative virions.

individual virions of VSV:eGFP-P, which represents variations in the number of P-eGFP packaged. The average fluorescence signal for 15 virions was 1233 ± 351 photons. As shown in Fig. 2D, virions with fewer eGFP-P copies showed the largest displacement of the eGFP localization with respect to the center of the virion, while virions with the maximum number of eGFP-P copies had almost no displacement. The linear relationship between the displacement and the number of packaged eGFP-P molecules shown in Fig. 2D indicates a constant packing density of P proteins as they fill the cavity starting from the blunt end. In average the center of mass of the P-eGFP was displaced from the center of the virion by a distance of 50 ± 21 nm.

Because P proteins associate with L, we next measured the distribution of L. We also found variation in the fluorescence signal between individual VSV:L-eGFP virions of 461 ± 202 photons. Furthermore, as with the eGFP-P, we observed a linear relationship between the L-eGFP fluorescence intensity and the displacement of

the fluorescence center from the virus center as shown in Fig. 2F. Again, this indicates uniform packaging of L-eGFP proteins at the blunt end of the virus. The average center of fluorescence for 20 VSV:L-eGFP virions was located 46 ± 22 nm from the geometric center of the virus toward the blunt end. We conclude that P and L package asymmetrically the same volume at the blunt end of VSV.

Note that neither VSV:eGFP-P nor VSV:L-eGFP package wild type levels of L and P (see below), so the fluorescent measurements cannot be used to estimate either the density or the exact length of the volume in which L and P package in wild type virions.

3.2. AFM reveals protein density at the blunt end of VSV

We next used a fluorescence-free assay both to corroborate the above results and to estimate the size of the volume occupied by L and P proteins within wild type virions. Any variation in the

protein density along the length of a virus particle should lead to a change in its mechanical properties, specifically its stiffness. Stiffness of the envelopes viruses [18] is almost an order of magnitude less than non-enveloped viruses like bacteriophage [20] or adenovirus [27]. The proteins associated with the envelope of VSV (G, M and N) have a symmetric helical organization [3], therefore, the AFM tip can deform the envelope and probe the stiffness of the underlying structure which should have no variance along the central axis of the virus. Internal proteins and genomic structure of the viruses have direct effects on their mechanical properties, as shown previously for DNA binding within the capsid of parvovirus of mice [28] and maturation of HIV virions [18,29]. We hypothesized that the virus should be stiffer at the blunt end due to the presence of an over density of P and L proteins there. Using a relatively stiff cantilever with tapping-mode AFM under ambient conditions, we performed an iso-force scan of the virions tethered on glass surfaces as explained in the methods. The stiffness measurements rely on using the AFM probe as a force sensor. In particular for soft samples, the probe depresses the surface, and the degree of depression is related to the stiffness of the sample relative to the spring constant of the AFM cantilever (SI). We were able to press considerably into the virus and detected an increase in the height of the virus at the blunt end. Since the scans are iso-force, the increase in height indicates an increase in stiffness from extra protein density at the blunt end. AFM was able to resolve the asymmetric bullet shape of the virions, thus placing the region of elevated stiffness at the blunt end (Fig. 3 and SI).

As shown in Fig. 3, we observed virions with 180×80 nm bullet shapes, each with recognizable tapered and blunt ends distinguished by analyzing the AFM cross sections (SI). During AFM scans, the tip locally compresses the virions to a height of ~ 30 nm due to deformation of the soft viral envelope, but the measured widths (~ 100 nm) accurately reflect the true diameter of the virions with a 20 nm convolution. This demonstrates that the virions were not “pancaked” onto the substrate due to surface interactions or dehydration. This was confirmed by increasing the force and pushing the virus into the non-elastic region which resulted in fully deformed virions (data not shown).

For all wild type virions measured, there was a region at the blunt end that exhibited less depression (higher stiffness) compared to the rest of the virus, as shown in green. This region extended 57 ± 12 nm in length from the blunt end, obtained from a sample of 50 wild type viruses.

3.3. Detected density at the blunt end of the virus correlates with the amount of P and L packaged

Recombinant VSV:eGFP-P viruses exhibit slower than wild type growth kinetics and package about half the number of P and L proteins compared to the wild type. Their bullet-shaped morphology is, however, indistinguishable from the wild type when viewed in EM [23,30]. For 30 VSV:eGFP-P virions, the region of higher stiffness extended 68 ± 21 nm, but the magnitude of elevated stiffness was much lower compared to wild type, as shown in Fig. 3. These results suggest that VSV:eGFP-P forms a protein complex of lower density compared to the wild type. A GFP-labeled P cannot package as densely as wild type because eGFP likely sterically hinders packaging. This may explain why the eGFP-P virions have a volume with lower stiffness than wild type that nonetheless extends significantly within the cavity.

VSV:L-eGFP viruses are only partially functional, package only about a third as much L as wild type (but normal amounts of P), and do not transcribe their RNA *in vitro*. They do, however, replicate well at 32 °C and form VSV virions with the correct morphology [24]. Increased stiffness at the blunt end of VSV:L-eGFP was

almost undetectable via AFM, consistent with a much lower density volume of polymerase complexes compared to wild type.

4. Discussion

Using high-resolution fluorescence imaging and center of mass calculations on recombinant viruses in which all wild type L or P proteins were genetically replaced with GFP linked fusion proteins of L and P, we show asymmetric packaging of the polymerase complex of VSV at its blunt end. L and P packaged within the blunt end of the virus create a region of higher stiffness within the blunt end of the virus. We measured this region of higher stiffness using AFM and in WT virions report its average length at 57 nm with a variation of ± 12 nm among virions. This variation reflects the variable number of L and P packaged in each virion as also measured with fluorescence and shown in Fig. 2.

The present study has focused on identifying the position of the polymerases within the cavity of VSV which resulted in identifying the asymmetric distribution of polymerases at the blunt end of the virus. Transcription of the virion N-RNA is the first step required for virus multiplication after entry into the host cytosol, and this can only initiate at or near the 3' end [21,22]. Recent CryoEM studies showed the N-RNA winds around a cavity in a left-handed helix, starting with its 3' end at the virus's tapered end and culminating with the 5' end at the blunt end of the virus [2,3]. Based on our observations, the polymerases are therefore stacked at the 5' end of the genome rather than at the 3' end where the transcriptional promoter is located. We envision two ways in which the polymerase units can reach the 3' transcriptional promoter. In the first model, we hypothesize it would be possible to start transcription through formation of an N-RNA template loop that brings the 3' end of the genome close to the 5' end of the N-RNA where the polymerases are located. Such N-RNA loops have been identified in the cytoplasm of cells infected with VSV before [31]. The observed asymmetry of the polymerase localization along the genome however cannot rule out the traditional model of transcription in which L-P_x complexes dissociate from the N-RNA and re-engage the promoter at the 3' end.

Acknowledgments

We thank Prof. Stephen Harrison for fruitful discussions and comments in preparation of this manuscript, Prof. Sean Whelan for VSV:PeGFP virus and Jeff Ballew for providing support and technical assistant. This work was supported by NSF grants 1121972 (S.S.) and DBI-0845193 (J.M.G.).

Appendix A. Supplementary data

Supplementary data associated with this article can be found, in the online version, at <http://dx.doi.org/10.1016/j.bbrc.2013.09.064>.

References

- [1] S.J. Russell, K.W. Peng, J.C. Bell, Oncolytic virotherapy, *Nat. Biotechnol.* 30 (2012) 658–670.
- [2] T.J. Green, X. Zhang, G.W. Wertz, M. Luo, Structure of the vesicular stomatitis virus nucleoprotein–RNA complex, *Science* 313 (2006) 357–360.
- [3] P. Ge, J. Tsao, S. Schein, T.J. Green, M. Luo, Z.H. Zhou, Cryo-EM model of the bullet-shaped vesicular stomatitis virus, *Science* 327 (2010) 689–693.
- [4] A. Desfosses, E.A. Ribeiro, G. Schoehn, D. Blondel, D. Guilligay, M. Jamin, R.W.H. Ruigrok, I. Gutsche, Self-organization of the vesicular stomatitis virus nucleocapsid into a bullet shape, *Nat. Commun.* 4 (2013) 1429.
- [5] I. Ivanov, F. Yabukarski, R.W.H. Ruigrok, M. Jamin, Structural insights into the rhabdovirus transcription/replication complex, *Virus Res.* 162 (2011) 126–137.
- [6] H.R. Jayakar, E. Jeetendra, M.A. Whitt, Rhabdovirus assembly and budding, *Virus Res.* 106 (2004) 117–132.
- [7] B. Morin, P.J. Kranzusch, A.A. Rahmeh, S.P.J. Whelan, The polymerase of negative-stranded RNA viruses, *Curr. Opin. Virol.* 3 (2013) 103–110.

- [8] A.A. Rahmeh, B. Morin, A.D. Schenk, B. Liang, B.S. Heinrich, V. Brusic, T. Walz, S.P.J. Whelan, Critical phosphoprotein elements that regulate polymerase architecture and function in vesicular stomatitis virus, *Proc. Natl. Acad. Sci. USA* 109 (2012) 14628–14633.
- [9] A.A. Rahmeh, A.D. Schenk, E.I. Danek, P.J. Kranzusch, B. Liang, T. Walz, S.P.J. Whelan, Molecular architecture of the vesicular stomatitis virus RNA polymerase, *Proc. Natl. Acad. Sci. USA* 107 (2010) 20075–20080.
- [10] H. Ding, T.J. Green, S. Lu, M. Luo, Crystal structure of the oligomerization domain of the phosphoprotein of vesicular stomatitis virus, *J. Virol.* 80 (2006) 2808–2814.
- [11] I. Ivanov, T. Crépin, M. Jamin, R.W.H. Ruigrok, Structure of the dimerization domain of the rabies virus phosphoprotein, *J. Virol.* 84 (2010) 3707–3710.
- [12] R.E. Thompson, D.R. Larson, W.W. Webb, Precise nanometer localization analysis for individual fluorescent probes, *Biophys. J.* 82 (2002) 2775–2783.
- [13] M. Kaksonen, D.G. Drubin, PALM reading: seeing the future of cell biology at higher resolution, *Dev. Cell* 11 (2006) 438–439.
- [14] S.T. Hess, T.P.K. Girirajan, M.D. Mason, Ultra-high resolution imaging by fluorescence photoactivation localization microscopy, *Biophys. J.* 91 (2006) 4258–4272.
- [15] M.J. Rust, M. Bates, X.W. Zhuang, Sub-diffraction-limit imaging by stochastic optical reconstruction microscopy (STORM), *Nat. Methods* 3 (2006) 793–795.
- [16] B. Huang, W. Wang, M. Bates, X. Zhuang, Three-dimensional super-resolution imaging by stochastic optical reconstruction microscopy, *Science* 319 (2008) 810–813.
- [17] M.F. Juette, T.J. Gould, M.D. Lessard, M.J. Mlodzianoski, B.S. Nagpure, B.T. Bennett, S.T. Hess, J. Bewersdorf, Three-dimensional sub-100 nm resolution fluorescence microscopy of thick samples, *Nat. Methods* 5 (2008) 527–529.
- [18] N. Kol, Y. Shi, M. Tsvitov, D. Barlam, R.Z. Shneck, M.S. Kay, I. Rousso, A stiffness switch in human immunodeficiency virus, *Biophys. J.* 92 (2007) 1777–1783.
- [19] J. Snijder, V.S. Reddy, E.R. May, W.H. Roos, G.R. Nemerow, G.J.L. Wuite, Integrin and defensin modulate the mechanical properties of adenovirus, *J. Virol.* 87 (2013) 2756–2766.
- [20] M. Hernando-Pérez, R. Miranda, M. Aznar, J.L. Carrascosa, I.A.T. Schaap, D. Reguera, P.J. de Pablo, Physical virology: direct measurement of phage phi29 stiffness provides evidence of internal pressure (*Small* 15/2012), *Small* 8 (2012) 2365.
- [21] L.E. Iverson, J.K. Rose, Localized attenuation and discontinuous synthesis during vesicular stomatitis virus transcription, *Cell* 23 (1981) 477–484.
- [22] S.P.J. Whelan, G.W. Wertz, Transcription and replication initiate at separate sites on the vesicular stomatitis virus genome, *Proc. Natl. Acad. Sci. USA* 99 (2002) 9178–9183.
- [23] D.H. Schott, D.K. Cureton, S.P. Whelan, C.P. Hunter, An antiviral role for the RNA interference machinery in *Caenorhabditis elegans*, *Proc. Natl. Acad. Sci. USA* 102 (2005) 18420–18424.
- [24] J.B. Ruedas, J. Perrault, Insertion of enhanced green fluorescent protein in a hinge region of vesicular stomatitis virus μ polymerase protein creates a temperature-sensitive virus that displays no virion-associated polymerase activity *in vitro*, *J. Virol.* 83 (2009) 12241–12252.
- [25] W.I. Sundquist, H.-G. Kräusslich, HIV-1 assembly, budding, and maturation, *Cold Spring Harb. Perspect. Med.* 2 (2012).
- [26] J.A.G. Briggs, H.-G. Kräusslich, The molecular architecture of HIV, *J. Mol. Biol.* 410 (2011) 491–500.
- [27] A. Ortega-Esteban, A.J. Perez-Berna, R. Menendez-Conejero, S.J. Flint, C.S. Martin, P.J. de Pablo, Monitoring dynamics of human adenovirus disassembly induced by mechanical fatigue, *Sci. Rep.* 3 (2013).
- [28] C. Carrasco, A. Carreira, I.A.T. Schaap, P.A. Serena, J. Gómez-Herrero, M.G. Mateu, P.J. de Pablo, DNA-mediated anisotropic mechanical reinforcement of a virus, *Proc. Natl. Acad. Sci. USA* 103 (2006) 13706–13711.
- [29] H.-B. Pang, L. Hevroni, N. Kol, D. Eckert, M. Tsvitov, M. Kay, I. Rousso, Virion stiffness regulates immature HIV-1 entry, *Retrovirology* 10 (2013) 4.
- [30] S.C. Das, A.K. Pattnaik, Role of the hypervariable hinge region of phosphoprotein p of vesicular stomatitis virus in viral rna synthesis and assembly of infectious virus particles, *J. Virol.* 79 (2005) 8101–8112.
- [31] C.W. Naeve, D.F. Summers, Electron microscopy of vesicular stomatitis virus replicative ribonucleoproteins, *J. Virol.* 34 (1980) 764–771.

Supplementary Information for Asymmetric packaging of polymerases within vesicular stomatitis virus

Materials and Methods

Super-resolution fluorescence imaging sample preparation

Cleaning: Glass coverslips (Electron Microscopy Services Cat.#72225-01) were prepared in a clean room. Using a Teflon rack the coverslips were submerged in 95% ethyl alcohol, sonicated for 30 minutes, rinsed 4 times in 500mL of MilliQ water, placed in 10M NaOH, and sonicated again for 30 minutes. Using forceps, each coverslip was rinsed under stream of MilliQ water for 30-60 seconds and then stored in MilliQ water.

Glass chemistry: Clean coverslips were dried under a nitrogen stream before addition of chemistry. First, 25 μ L of biotinylated PEG (SuSoSPLL(20)-g[3.5]-PEG(2)/PEG(3.4)-Biotin (20%) at 0.5mg/mL in PBS) was placed onto a horizontally mounted coverslip. A second cleaned and dried coverslip was placed on top to form a sandwich and left for 45 minutes at room temperature. After incubation, the glass is separated and the "active face" was rinsed twice with 25mL of MilliQ water and allowed to dry for 45 minutes. For optimal results, PEG-ylated glass was used within 24 hours. Next, 25 μ L of a NeutrAvidin (Invitrogen NeutrAvidin biotin-binding protein A2666, 0.25mg/mL in PBS) was sandwiched between two active faces, incubated for 30 minutes, and rinsed four times with 25mL of MilliQwater. Immediately after NeutrAvidin treatment, 25 μ L of biotinylated antibody solution (α -VSV-G Invitrogenab34774, 1:200 in 0.2M KPO₄, 0.15M NaCl, 10%Glycol,pH 7.2 buffer) was sandwiched, incubated for 60 minutes, and rinsed four times with 25mL of cold 10mM HEPES pH 7.4. Immediately after antibody treatment, 25 μ L of prepared virus (see below) was sandwiched, incubated for 60 minutes, and rinsed four times with 25mL of cold 10mM HEPES pH 7.4.

Virus labeling: To label the virus, the active faces were sandwiched with 25 μ L of a primary antibody (α -VSV-G rabbit [invitrogen AB34774], 1:400) incubated for 30 minutes, and rinsed four times with 25mL of cold 10mM HEPES pH 7.4. Following the primary antibody, 25 μ L of a secondary antibody (Alexa Fluor®647 goat anti-rabbit IgG, Invitrogen A21245) was sandwiched, incubated for 30 minutes, and rinsed four times with 25mL of cold 10mM HEPES pH 7.4.

Virus preparation

Plaque purified VSV:eGFP-P (37C) and VSV:L-eGFP (32C) were grown and purified according to the following protocol:

90% Confluent BHK-21 cells were inoculated with VSV at an MOI of 3 in DMEM containing 2% FBS, 1X PKS and 10mM HEPES (pH 7.4). The medium was extracted the next day and cell debris was removed by centrifugation at 3000 rpm for 5min. After the spin the supernatant was filter clarified through a 0.4 μ m filter to remove any additional cellular debris resulting from cell lysis. Virus was then pelleted by centrifugation at 40,000 x g for 90 minutes @ 4°C. Virus pallet was re-suspended in NTE (10 mM Tris pH 7.4, 100 mM NaCl, 66 mM EDTA) on ice overnight. This solution was further purified through pelleting through a 10% sucrose cushion spin at 157,000 x g for 1h @ 4°C. The virus pellet was re-suspended in NTE on ice overnight. This solution was further purified through a 15%-45% Sucrose gradient spin at 79,000 x g for 3.5hrs. The virus was extracted at the boundary of the 45% sucrose using a syringe. The final virus prep was dialyzed against NTE overnight to dilute the extra sucrose.

HIV-1 VLP Purification

HIV-1 VLPs pseudotyped with VSV-G were produced in 293T cells (3×10^6 cells in 100 mm plates) by co-transfection (Fugene-HD, Roche) of the following plasmids: 7.5 μg of HIV-1 Gag (11-071), 1.5 μg HIV-1 Gag-eGFP (11-075) and 2.4 μg VSV-G (11-041). The medium was replaced 8 hours after transfection, and the supernatant was harvested 32 hours later and syringe-filtered through 0.45 μm membranes. VLPs were collected by pelleting 5 mL of the filtered medium through a 1 ml 20% sucrose in PBS cushion (centrifuge, 4°C, 2 hour, 40,000 RPM). The supernatant was removed and the pellet was re-suspended in 500 μL NTE (10 mM Tris-HCl, pH 7.4, 100 mM NaCl, 1 mM EDTA). To remove residual sucrose before imaging, the virus sample was treated by dialysis (Slide-A-Lyzer, mini dialysis unit; 10,000 MWCO, Thermo Scientific) at 4°C against NTE plus 10 mM HEPES.

VSV:G-eGFP Preparation

293 cells were plated a day before experiments and transfected using (Fugene-HD, Roche) with VSVG-eGFP plasmid. Cells were then infected with VSV WT 12hr post transfection with an MOI of 3. Supernatant was collected 24 Hrs post infection and VSV virions were purified as described under virus preparation.

Imaging buffer preparation

A 10x Stock of Gloxy was prepared in advance by adding 1,688 active units (AU) Gluox and 14,040 AU Catalase into 1mL of 50 mM Tris with 10mM NaCl (pH 8.0) and mixed gently.

The imaging buffer was created just prior to imaging by adding 50 μL of 1M MEA and 100 μL of 10x Gloxy to 850 μL of stock buffer.

Materials:

Gluox: Glucose oxidase type seven from *Aspergillus* #G2133-250KU (Sigma)

Catalase: Catalase from Bovine liver C40-100mg (Sigma)

Stock Buffer: 50 mM Tris-HCL (pH 8.0) + 10mM NaCl + 10% glucose.

MEA: Cysteamine (MEA) #30070-10G (Sigma)

Imaging data selection criteria

There are several selection criteria for virions used in this study.

- 1) Only particles with >70% confidence (as determined by the Vutara software χ^2 minimization localization) are considered. This was to eliminate noise.
- 2) Both probes (Alexa 647 and eGFP) must have a clear signal that was visible in the data. This was typically seen in that both the green and red channels have an obvious particle to consider. This was to eliminate non-virion particles as a virion should have both signals.
- 3) Virions had to have 70% or more of the frames in the eGFP data capture with a signal above 70% confidence.
- 4) Virions had to have 500 or more unique Alexa 647 particles as determined above. This was to ensure the virion had enough data to properly recover the surface via isosurfacing
- 5) Virions with grossly abnormal sizes (200% larger than expected in any dimension) were eliminated from consideration. This typically eliminated virions that may have had too much surfactant nearby, which distorted the antibody labeling.

eGFP and photo-bleaching calibration

Even though eGFP data was collected for 500 frames, it was found that the eGFP signals typically bleached during this collection. So, for all virions that were selected, the first 50 frames were utilized where the variation due to photo-bleaching was minimized. The data for those 50 frames were fit to a linear function and corrected for photo-bleaching by adding the slope for intensity over time back into the intensities.

Data analysis and normalization methodologies

After selection, all eGFP signals were rotated such that the center of fluorescence for the fluorescence of the eGFP points and the center of fluorescence of the Alexa 647 points lay along the X axis using an $e^{i\theta}$ rotation about the Alexa647 center of fluorescence as a pivot point. All virions were rotated such that the eGFP was to the right of the Alexa647. This rotation demonstrated that the offset existed along the principal axis of the virion and that each of the three virion types had differing average offsets. The histogram distribution of VSV eGFP-P intensity as well as VSV L-eGFP is presented in Figures S2&3

Super resolution control experiments

Bead data was used to determine the accuracy of the Biplane as shown below. The precision of localization is inversely proportional to the square root of the collected photon counts. The laser intensity was lowered on the bead samples such that the beads were matched to the typical photon count from the Alexa 647 in order to demonstrate our resolution. Below we present two sets of data, one where the photon counts are around 2000 and a lower bound where the photon counts are around 500.

Bead 1 Statistical Analysis to determine fPALM/STORM xyz localization precision on the SR-200 super-resolution microscope. For all the bead particles captured in the images, the x, y and z position was computed through localization analysis. The data from these 1000 localizations is presented for a representative bead in Figure S1. For each bead, statistical analysis was performed to determine the standard deviation of the positions over 1000 frames. Similar analysis was performed for all five beads and the results tabulated in Table S1.

We also performed mean and standard deviation statistical analysis on the individual 1000 positions obtained for seven beads, each intensity approximately equivalent to 2000 photons, in order to match our standard case. The mean and standard deviation (which is defined as the localization accuracy) was computed and tabulated below.

HIV co-localization control experiment

To confirm our ability to determine co-localization of eGFP signal within a viral envelope, we tested VSV-G pseudotyped HIV virus-like particles (VLP), in which a portion of HIV-Gag is tagged with eGFP. To image HIV VLPs, the same protocols for VSV experiments were used. For HIV VLPs, both Gag and VSV-G should be evenly distributed within the envelope and the signals are expected to co-localize. We observed a small shift of $12 \text{ nm} \pm 6 \text{ nm}$ which was within

our 20nm positional uncertainty (Table S2). When comparing the intensity to the offset, we see that there was a low correlation between offset and intensity (Fig. S4).

AFM Materials and Methods

AFM information:

Atomic Force Microscope(model): Asylum MFP-3D

Software version : 101010+1725

Mode of scan : AC air topography

Tip information:

All the data we took using Budget Sensors probes (Multi75GB) .

Tip radius <25nm

Application: force modulation, light tapping.

force constant: 3N/m.

Resonant frequency 75 KHz with uncertainty of 15 KHz

AFM Sample Preparation:

Sample preparation for AFM was identical to super-resolution fluorescence imaging sample preparation except AFM coverslip (AFM: Fisherbrand Microscope Cover Glass: 35 CIRCLE #1) were used. For the sandwich method, AFM coverslips required 40 μ L of fluid during each stage. AFM sample preparation was complete after virus laydown.

Blunt end versus Tip identification.

AFM data is captured using an isoforce method maintaining the virion in an elastic region as shown in Figure S6. These scans were used to deconvolve the virion surface based on the numerical deconvolution¹⁻⁴.

Identification of the tapered end vs. blunt end of VSV virions in both wild-type (WT) and P-eGFP mutants was accomplished by analyzing the curvature of the deconvolved scans, these curvatures showed a clear prolate region identifying the tip of the virion. We determined this by considering only the top half of the normalized curves in order to calculate ellipticity, all curves were fit with a sixth power polynomial function (with $R^2 > 0.999$ in all cases), and these fits can be categorized into two distinct groups of prolate (where the first plateau > 40nm) or oblate (where the first plateau < 40nm) ellipsoidal topology. In this idealized model, we note that the traditional rounded tip of VSV is described as prolate, while the blunt end can be described as oblate.

The bump region within the viruses (which is the plateau region corresponding to the volume occupied by L and P) is clearly separated from the plateau region corresponding to the empty helical region of the virus. On the virion shown in the Figure S6 B, the main body plateau standard deviation of height is 0.21 nm from a linear average, with a bump height of 1.56 nm above the main body. On average, across all virions, the standard deviation of height in the main body plateau is 0.83nm with an average height difference of 5.5nm. Thus the separation of these two plateaus are several standard deviations in height (typically ~ 7). clearly identifying these regions on the WT and P-eGFP virions.

The position of the bump which identified with the volume occupied by L and P was then scored versus the oblate or prolate geometry. 75 out of 80 virions analyzed showed the bump associated with the oblate geometry, one case had the bump associated with the prolate side of the virion and in 4 cases the oblate and prolate curvatures were difficult to distinguish. This data strongly correlates the presence of the bump associated with the volume occupied by L and P at the blunt end of the virus.

References

- 1 Thompson, R. E., Larson, D. R. & Webb, W. W. Precise Nanometer Localization Analysis for Individual Fluorescent Probes. *Biophys. J.* **82**, 2775-2783 (2002).
- 2 Rust, M. J., Bates, M. & Zhuang, X. W. Sub-diffraction-limit imaging by stochastic optical reconstruction microscopy (STORM). *Nature Methods* **3**, 793-795 (2006).
- 3 Betzig, E. *et al.* Imaging intracellular fluorescent proteins at nanometer resolution. *Science* **313**, 1642-1645 (2006).
- 4 Hess, S. T., Girirajan, T. P. K. & Mason, M. D. Ultra-High Resolution Imaging by Fluorescence Photoactivation Localization Microscopy. *Biophys. J.* **91**, 4258-4272 (2006).
- 5 Juetten, M. F. *et al.* Three-dimensional sub-100 nm resolution fluorescence microscopy of thick samples. *Nat Meth* **5**, 527-529, doi:http://www.nature.com/nmeth/journal/v5/n6/supinfo/nmeth.1211_S1.html (2008).
- 6 Mlodzianoski, M. Sample drift correction in 3D fluorescence photoactivation localization microscopy. *Optics Express* **19**, 15009-15019 (2011).
- 7 Courant, R. & John, F. *Introduction to Calculus and Analysis*. Vol. 2 (John Wiley and sons, 1974).
- 8 Lorensen, W. E. & Cline, H. E. in *Proceedings of the 14th annual conference on Computer graphics and interactive techniques* 163-169 (ACM, 1987).
- 9 Johnson, K. L. *Contact mechanics*. (Cambridge University Press, 1985).
- 10 Popov, V. L. *Contact Mechanics and friction: Physical principles and applications*. (Springer Heidelberg, 2002).
- 11 Wriggers, P. L. T. A. *Computational Contact Mechanics*. . (Springer Wein 2007).
- 12 Hughes, J. E. M. a. T. J. R. *Mathematical Foundations of Elasticity*. (Dover Publications Inc., 1994).

Figures:

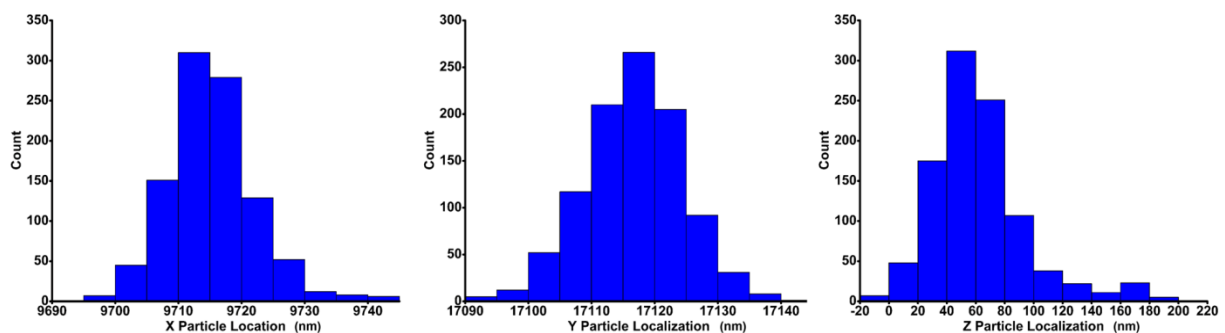


Figure S1 Statistical analysis of Bead 1 fluorescence distribution showing that over 1000 frames of collected data the variation in location X,Y,Z was 5nm, 7nm, 21nm respectively. Additionally there was a FWHM in X,Y, Z of 13nm, 17nm, and 51nm respectively.

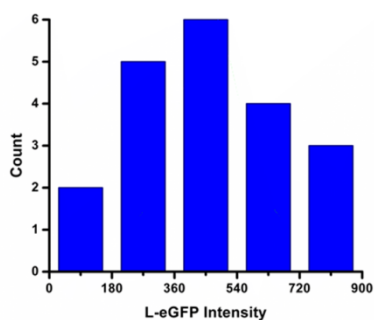


Figure S2 Histogram of the intensity distributions for VSV L-eGFP.

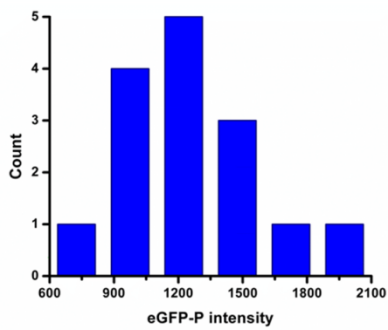


Figure S3 Histogram of intensity distributions for VSV eGFP-P.

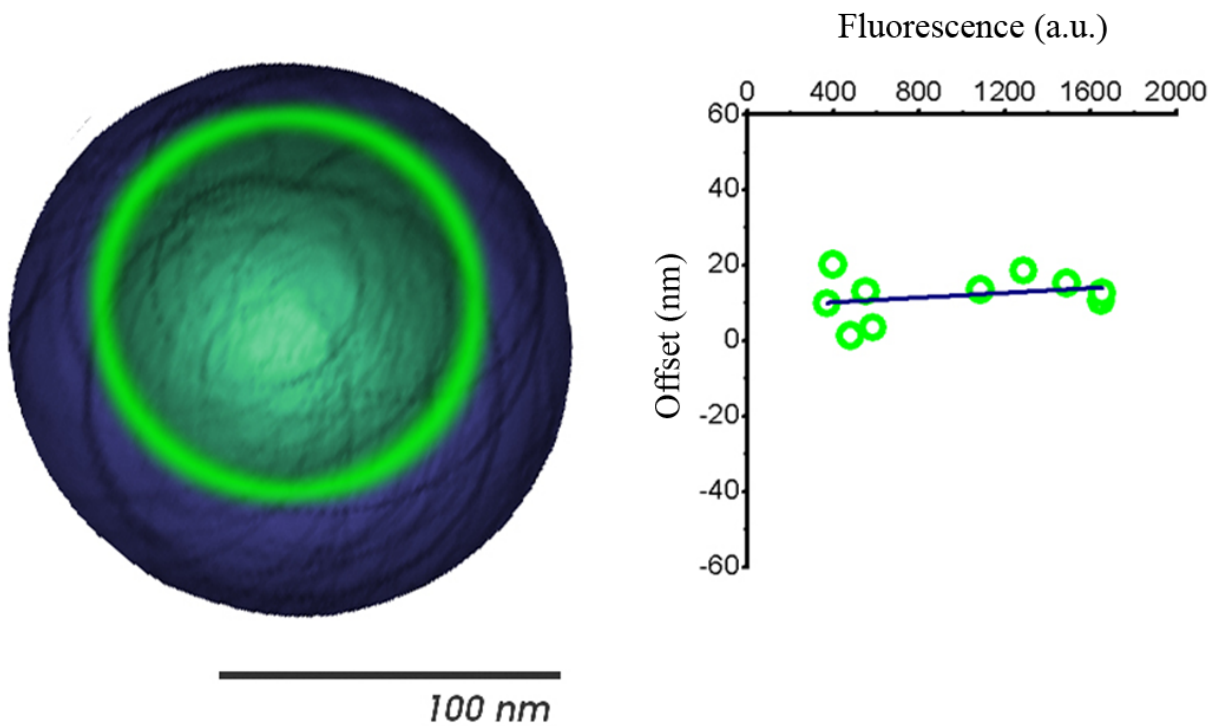


Figure S4 Shown on left: An isosurface of the colocalization of pseudotyped HIV GAG eGFP with VSVG and Alexa 647. Shown on right: GFP intensity vs. Offset which shows a low correlation ($R^2 = 0.0798$) between the two when fit linearly.

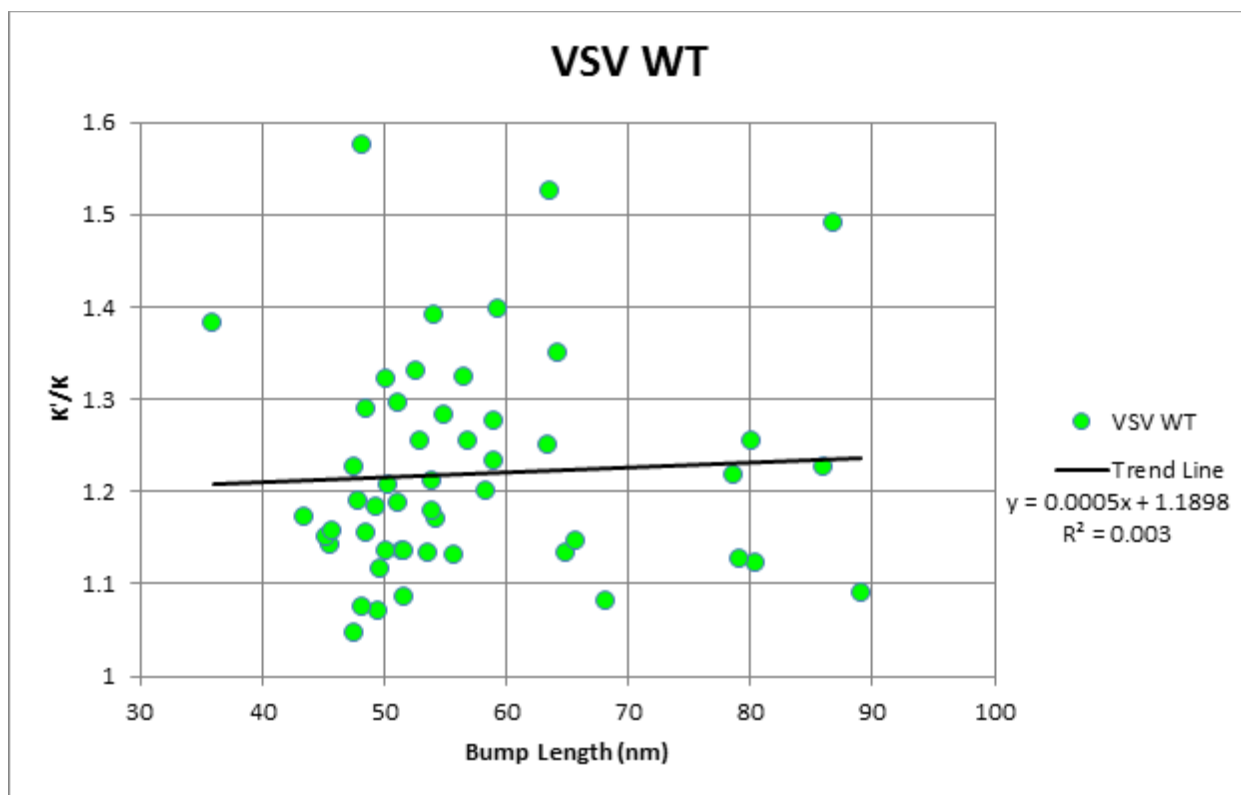


Figure S5: Scatter plot of the relationship between K'/K and bump length shown there is no correlation ($R^2 = 0.003$).

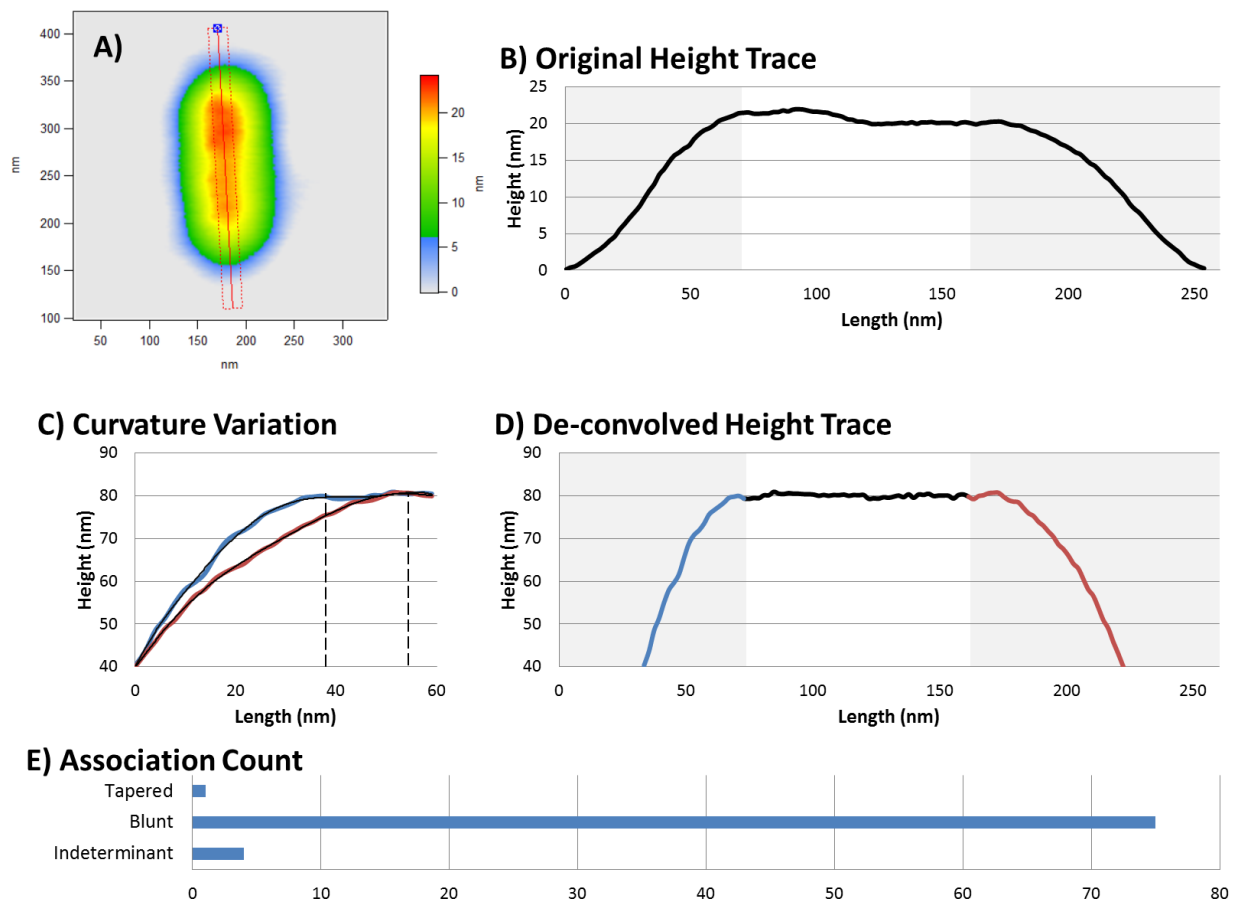


Figure S6 Deconvolution analysis for virions was accomplished by analyzing the central axis A). In this region there is little or no XY convolution due to the tip. The only convolution is in Z, B) Shows a height trace along the axis highlighted in A. Both the original trace (B) and the deconvolved height trace (D) show a significant variance in curvature from one side to the other. C) The curvatures from the two end of the virion are plotted together to Show a comparison of curvatures from the same virion, one curvature is distinctly prolate (shown in red) and is associated with the tapered end of the virion. E) Scoring of the bump position with the identified blunt end of the virion through oblate curvature of the scan (shown in blue in (C and D).

Tables:

| | x | | y | | z | | Average number of photons |
|--------|-----------|-----------------------------|-----------|-----------------------------|-----------|-----------------------------|---------------------------|
| | FWHM (nm) | Localization Precision (nm) | FWHM (nm) | Localization Precision (nm) | FWHM (nm) | Localization Precision (nm) | |
| Bead 1 | 13 | 5 | 17 | 7 | 51 | 21 | 667 |
| Bead 2 | 20 | 8 | 21 | 9 | 76 | 32 | 459 |
| Bead 3 | 16 | 7 | 16 | 7 | 52 | 22 | 655 |
| Bead 4 | 16 | 7 | 17 | 7 | 60 | 25 | 510 |
| Bead 5 | 15 | 6 | 17 | 7 | 47 | 20 | 572 |

Table S1 Localization precision in nm for five sample beads showing standard deviations of 9 nm or less with a FWHM of 21 nm or less in all X,Y. For Z, we find a localization precision of 32 nm or less and a FWHM of 76nm or less. The average capture time was corrected to have a similar photon count to our worst virions, around 572 photons per frame.

| | x | | y | | z | |
|--------|-----------|-----------------------------|-----------|-----------------------------|-----------|-----------------------------|
| | FWHM (nm) | Localization Precision (nm) | FWHM (nm) | Localization Precision (nm) | FWHM (nm) | Localization Precision (nm) |
| Bead 1 | 15 | 6 | 12 | 5 | 51 | 21 |
| Bead 2 | 14 | 6 | 13 | 5 | 52 | 22 |
| Bead 3 | 18 | 7 | 14 | 6 | 41 | 17 |
| Bead 4 | 16 | 6 | 14 | 6 | 62 | 26 |
| Bead 5 | 14 | 6 | 13 | 5 | 37 | 15 |
| Bead 6 | 14 | 6 | 13 | 5 | 54 | 23 |
| Bead 7 | 16 | 6 | 17 | 7 | 43 | 18 |

Table S2 Table of localization precision and FWHM measurements for 7 beads with approximately 2000 photon counts to match our standard case.

- 1 Johnson, K. L. *Contact mechanics*. (Cambridge University Press, 1985).
- 2 Popov, V. L. *Contact Mechanics and friction: Physical principles and applications*. (Springer Heidelberg, 2002).
- 3 Wriggers, P. L. T. A. *Computational Contact Mechanics*. . (Springer Wein 2007).
- 4 Hughes, J. E. M. a. T. J. R. *Mathematical Foundations of Elasticity*. (Dover Publications Inc., 1994).